Variational decompression of image data from DjVu encoded files

Martin Holler, Kamil S. Kazimierski

***Abstract*—The DjVu file format and image compression techniques are widely used in the archival of digital documents. Its key ingredients are the separation of the document into fore- and background layers, followed by a lossy, transform based compression of the former and a dictionary based compression of the latter. The lossy compression of the layers is based on a wavelet decomposition and bit truncation, which leads, in particular at higher compression rates, to severe compression artifacts in the standard decompression of the layers.**

In this paper we propose a novel decompression method for DjVu images which eliminates compression artifacts in fore- and background layers, while at the same time preserving main geometrical properties like smooth gradients and sharp edges. Our method is based on the combination of data constraints obtained by a thorough analysis of the DjVu compression procedure and the Total Generalized Variation (TGV) functional as image model. It is formulated as convex constrained optimization problem and an efficient algorithmic implementation allowing to obtain provably optimal solutions is provided. Numerical experiments demonstrate a significant improvement of image quality compared to both standard decompression as well as different post-processing strategies.

I. Introduction

THE aim of this paper is to provide a novel and improved decompression technique for DjVu files. Our approach is based on a mathematical modeling of expected image structures via an appropriate regularization functional and the minimization of this functional subject to constraints that are obtained from the compressed DjVu file. The latter requires a thorough analysis of the DjVu compression procedure, whose detailed description can be seen as supplementary contribution of the paper.

The DjVu standard generally is designed for handling the document to be compressed in three different layers, a fore- and background layer and a binary switching mask. While the compression of the mask is achieved mainly by exploiting repeating patters, such as letters, with a dictionary-based encoding, compression of the layers relies on a deliberate loss of data that is less relevant image quality. This is done essentially via a wavelet transform and subsequent bit truncation, which leads, at higher compression levels, to strongly visible artifacts in the images. Our approach is focused on inverting the compression of these layers.

Compression of the fore and background layers in DjVu in general consists of two major steps: The first one comprises a color space transform, a subsequent wavelet decomposition of the resulting color channels and in a final part a decimation step, the latter being responsible for the 'lossy' property of the image compression. In a second step, an entropy based encoding is applied to the serialized data of the first step. This lossless part of the encoding is implemented via (context adaptive, binary) arithmetic coding. Within the decoding in mind, the only problematic part of the encoding chain is the decimation, since, obviously, there are many data which, when decimated, return the same result, i.e., the decimation is not an invertible process.

The standard decoding process in turn consists of an entropy decoding followed by an inverse wavelet transform and an inverse color transform. Virtually, the decimation step of the encoding is ignored, and the truncated wavelet coefficients are taken as the ground truth. This choice, however, is somewhat arbitrary, in particular it is carried out regardless of any additional information on the geometric properties of the image. In contrast to that, the main methodological concept of this paper is to incorporate such properties into the inversion of the decimation.

Within the encoding/decoding chain, the entropy decoding and the color transform can be regarded as fixed pre- and post-processing steps of our approach. The color transform in DjVu (as is usual in image compression) is a pixel-wise/local and invertible transform. Therefore any local geometric properties of the image can be equivalently formulated in the original as well as in the color-transformed space. Further the entropy decoding can be done as precprocessing as it is assumed to be invertible too. These consideration lead to the following approach.

Variational image decompression scheme. First, the decimated wavelet coefficients (of the original image) are obtained by entropy decoding. Together with a coefficient-dependent decimation-strength parameter (which can be obtained from the file) this characterizes a set D of admissible undecimated wavelet coefficients, i.e., a set of images in the wavelet domain which - after decimation - have the same decimated wavelet coefficients as the original one. The main computational step is now to find an image for which the wavelet-transform lies in D and which at the same time admits a given image model optimally. Finally, from that optimal image (in the color space) an image (in the original space) is obtained by inverting the color transform.

Here, an image model is a way to differentiate among all (color-transformed) u the ones which are reasonable within a given application, i.e., desirable outputs of the decompression. Formally, such a model is formulated as a (typically non-negative) functional which is small only for desired images.

The DjVu file format is designed for the archival of documents. Therefore, typical images encountered in the image

Martin Holler and K. S. Kazimierski are with the Institute of Mathematics and Scientific Computing, Graz University, Austria. The Institute of Mathematics and Scientific Computing is a member of NAWI Graz (www.nawigraz.at) and BioTechMed Graz (www.biotechmed.at).

compression are either photographs or synthetic schematics like cartoons, plots, diagrams, maps or schematics. For such images, the Total Generalized Method (TGV) as proposed in [1] constitutes a good model and is therefore used in our approach.

Related work. There are, to the best knowledge of the authors, no other works available that approach DjVu decompression via variational modeling and optimization. Regarding the underlying problem structure of DjVu image decompression, however, variational JPEG 2000 decompression is closely related. Even tough the coefficient encoding and wavelet types are different, the optimization problem for variational DjVu image decompression itself is in fact a particular case of the general setting analyzed in [2], [3], dealing with applications to JPEG and JPEG 2000 decompression. Furthermore, the works [4], [5], [6], dealing with wavelet inpainting, cover a related setting and we provide a comparison to the approach of [5], which uses non-local TV regularization. More generally, considering DjVu image decompression as variational image dequantization in a basis-transform-domain, also variational JPEG decompression is related and we refer to [7], [8], [9] for comparable approaches. Independent of such conceptually related methods, however, we stress that the variational decompression of DjVu files requires to obtain the set of admissible wavelet coefficients from the actually encoded file, which is a non-trivial preprocessing step that has not been addressed by existing methods.

The remainder of the paper follows the model-based image decompression scheme described above. For the construction of the set D, a thorough knowledge of the DjVu format, in particular its serialization and decimation steps, is necessary. To the authors best knowledge this information is not available in the literature beyond the original format specification (cf. e.g. [10]). Therefore, for the sake of completeness, we provide a thorough overview over the specific properties of the DjVu format in the next section. Readers familiar with the format may skip that section. In Section III the TGV-based decompression scheme and the related optimization problem is described. In the subsequent section, an implementation, which is based on the Chambolle-Pock algorithm [11], for the solution of the optimization problem is proposed. The paper closes with a comparison of the proposed approach to other state-of-the-art methods.

II. DjVu

The DjVu image compression technology and file format was developed in the second half of the nineties [12]. A detailed specification of the pure image format (version 2) and the variously extended version 3 is available online at [13], [14]. An open reference implementation *djvulibre* is available at [10].

A DjVu file is a container based on the EA IFF 85 [15]. It consists of chunks aligned on 16-bit words. Beginning with version 3 the DjVu supports multi-page documents. On a structural level a single page consists of three principal parts, the foreground image, the background image and a mask indicating the foreground, see Figure 1. These parts can also

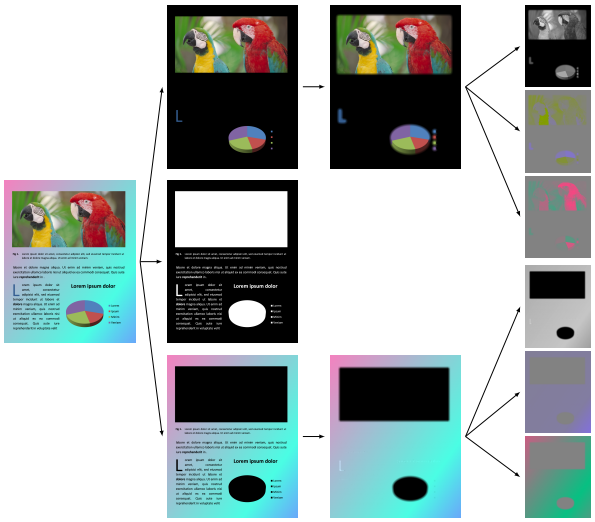

Fig. 1. Decomposition of a single DjVu page into layers and subsequent decomposition of layers into color channels.

be enriched by additional data like thumbnails, annotations or OCR data. In the simplest case, the foreground, background and mask parts of a page are raster images both having the same dimension as the page itself. The foreground and background can be either gray-scale or color images, whereas the mask is always bi-tonal. The foreground part depicts fine features of the page like figures, tables and text, whereas the background part consist of coarse parts of the page like paper structure or smooth background (e.g. color gradients). The mask is then used to locally switch between the foreground and the background image.

The DjVu specification allows for great flexibility in handling the three principal components. The mask can either be stored in DjVu native, lossless JB2 format or as CCIT Fax Group 4 (G4/MMR) image. The JB2 format decomposes the bi-tonal mask into a list/dictionary of smaller shapes. These shapes can then be encoded directly or as refinements of other shapes. Finally the dictionary is serialized and compressed by an DjVu native entropy coder (the so called ZP coder or Z' coder).

The foreground and background data can be either stored in the DjVu native IW44 format or as a JPEG image. It should also be noted that the DjVu image model of separating a single page into foreground, background and mask needs an appropriate segmentation, which the standard assumes to be given.

To summarize, while the concept of page separation into different layers reflects the focus of DjVu to scanned documents, the main ingredients of its compression performance are an efficient storage of the bi-tonal mask and the two image layers representing fore- and background information. For the latter, a loss of data is explicitly tolerated by using lossy transform based image encoding, which naturally leads to compression artifacts at higher compression rates. The focus of this work is to avoid such compression artifacts by using variational

methods to invert the lossy encoding of the image layers within the DjVu standard. We will focus on the DjVu native IW44 format for images, however, similar techniques can be carried out for JPEG images (see [2], [3]).

In a nutshell, the image information is stored via the coefficients of a wavelet representation with respect to the Dubuc-Deslauriers-Lemire (DDL) $(4,4)$ wavelets [16]. To achieve compression, the wavelet coefficients are re-ordered according to their expected importance for visual image quality, see Figure 2, and subsequently encoded via a bit-level-wise encoding stream, see Figure 3. This produces 200 so called slices, where each slice essentially contains the information of one bit level of a set of coefficients. The number of actually stored slices then defines the compression rate for the image. Obviously, due to the absence of some slices in the encoded DjVu file, the wavelet coefficients representing the image are known only with reduced precision, with the precision of each coefficient depending on its importance granted during the encoding process. The standard DjVu decoding process now estimates the full precision wavelet coefficients by taking the center of their admissible range defined by the low precision data. The image is then obtained by an inverse wavelet transform on these estimated coefficients.

On an abstract level, the information provided above suffices to understand the concept of our decompression approach, as described in Section III. However, to obtain the level of precision up to which each wavelet coefficient of each image layer is known from a given DjVu file, which is an essential ingredient of our method, a much more detailed understanding of DjVu is necessary. It is the goal of the following paragraphs to provide such an understanding. We will describe IW44-based DjVu image coding by elaborating the decompression procedure, which is split into *band decoding*, *wavelet reconstruction* and *color reconstruction*. But before that, it is essential to understand the data layout of the IW44 coefficients in terms of bands, which is described in the following

A. IW44 coefficient layout

The information of each image layer within a DjVu file is stored in terms of of the wavelet coefficients of the 5-level (DDL) $(4,4)$ wavelet transform of each color channel, where the color channels are represented in the YCbCr format that separates brightness and color information. To explain the layout of the wavelet coefficients of one color channel in more detail, new technical termini — block, band, bucket, slice and cycle — will be introduced and described in the following.

The main container for storage of wavelet coefficients is a block of 1024 coefficients representing roughly a patch of 32x32 pixels in the original image. The wavelet coefficients of a single block are selected as a set of spatially neighboring coefficients from all wavelet bands. The coefficients of each block are then grouped to 10 different bands, which are related but do not agree with the wavelet bands.

Every band is then subdivided into a variable number of so called buckets (i.e. containers of 16 coefficients). The first four bands have 1 bucket each, the following 3 bands consist of 4 buckets each and finally the last three bands have 16 buckets

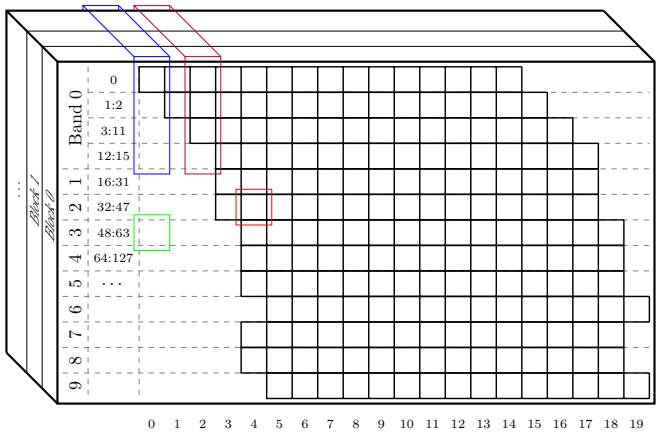

Fig. 3. Band-wise bit-slicing. A bitslice (colored highlights) are selected bits of coefficients within a selected band throughout all blocks of the image.

each. The partitioning of bands into buckets is relevant for the update of contexts in lossless encoding, as described in the next subsection, but will not be needed for the moment.

The above described *physical* partition of the wavelet coefficients of an image in blocks and bands is then used for a *logical* partition by means of bit-slicing. Each single wavelet coefficient is represented as a tuple of a 1-bit sign and 15-bit mantissa. (Notice that this is *not* equivalent to a 16-bit signed int as the number -2^{16} (the lowest value expressible as 16-bit signed int) cannot be represented in the 1+15 bit tuple form.) In order to be able to give less importance to some coefficients when employing a bit-level wise encoding, the 15 bits representing the coefficient magnitude are virtually extended to 20 bits, by introducing empty bit levels. A slice then encodes one bit level of one band of all blocks, e.g., slice 0 encodes the highest bit of all coefficients in the first band of all blocks, see Figure 3. As there exist 10 bands in each block and each coefficient has 20 (virtual) bit-levels, the bit-slicing generates 200 slices in total. Due to the ordering in which the coefficients contribute to the slices, the importance of slices for visual image quality is assumed to decrease for subsequent slices. Note also that, due to the virtual bit-levels, some slices are in fact always empty. The number of stored slices is the main compression parameter of the IW44 format.

Within the DjVu file, the streams of slices of all channels are stored in so called cycles (group of one slice for every channel). Doing so, the format also allows for a delay of both chroma channels with respect to the luminance channel. This delay is a second parameter which can be employed for compression purposes.

In general the cycles of an IW44 image may be distributed among several chunks of the DjVu file. As such, if needed, a further re-compression of a DjVu file can be obtained by deleting the last chunks of the background respectively of the foreground layer, without the need to implement the whole IW44 encoding-decoding scheme.

The overview of the main decoding loop is as follows: The image is decoded in cycles, which consist of the decoding of a given slice for every channel. Every slice is then decoded block

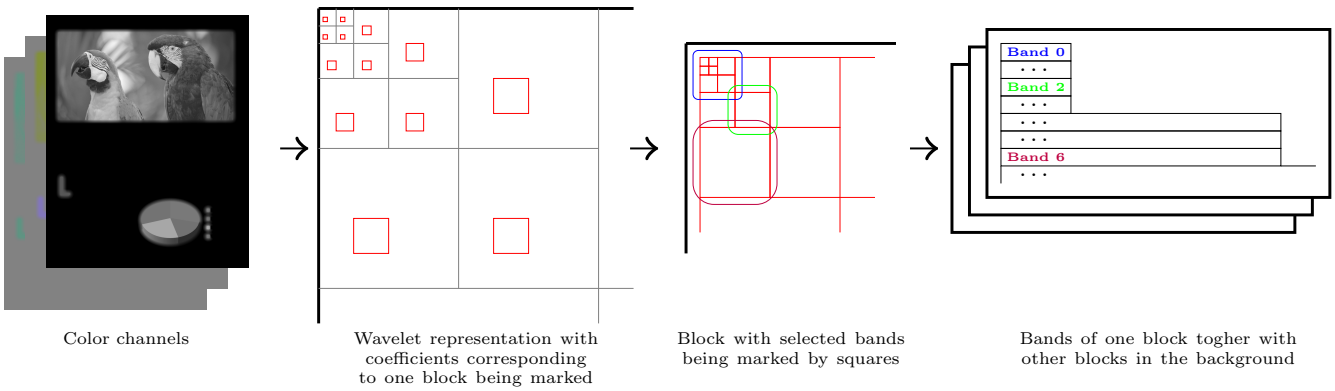

Fig. 2. Serialization layout for IW44 coefficients.

by block, i.e. in this step the decoding combines the logical partitioning with the physical partitioning of the image. Since a single slice always deals with one band of coefficients only, the decoding of a bit-slice for a band of coefficients within a single block is the main part of the decoding procedure.

B. Band decoding

Following the overview of the decoding loop as described above, this section deals with the decoding of a single bit slice of a given band of a single block of coefficients. To this aim, remember that each band is divided into 1, 3 or 16 buckets, each containing 16 coefficients. Accordingly, the bit slice decoding of a band is subdivided into a bit slice decoding of the coefficients of each bucket.

Now given the encoded bit stream corresponding to a bit slice of the current band, the decoder naturally has to interpret each bit of this stream. For storage and computation efficiency, the meaning of each bit depends on the current state of the partly decoded coefficients, buckets and bands. For example, depending on the state of the current bucket, a single bit of the stream can either encode that the current bit level of all coefficients in the bucket (having a certain state) contains 0, or it can encode the value of the current bit level of a single coefficient. To account for that, the decoder tracks the current state of each coefficient, bucket and band using *potential* and *active* flags.

Regarding these flags, first remember that each wavelet coefficient is represented as a tuple of a 1-bit sign and 15-bit mantissa. As explained in the last section (cf. also Figure 3) the bits of the mantissa are decoded beginning with the most significant bit down to the least significant bit. Within this process the sign bit is decoded together with most significant 1 bit. Consequently, no sign bit is decoded for the wavelet coefficient value of 0. A single coefficient at a current state is now called potential, if all bit-levels decoded so far contained only 0, i.e., the sign-bit has not yet been decoded. Otherwise, if already one 1 bit has been decoded, the coefficient is called active. Similarly, a bucket and band is set potential/active if it contains at least one potential/active coefficient. In contrast to the coefficients, the potential and active flags for buckets and bands can be set at the same time.

As initial step for decoding of a bit slice of the current band, all relevant coefficients are identified as active or potential. Further, all buckets and the band itself are marked as active and/or potential. The decoding is then carried out in four steps.

The first step deals roughly with the question if there are coefficients in the current band which will transition from potential to active in this band decoding. The answer to this question is stored in a flag. This flag is always set for bands 0-6. For bands 7-9, if the band is active the flag is set otherwise the flag is decoded from the bit stream at the current pointer position.

The second step is the analogue of the first step at the bucket level. If the flag from last step is set, then for every potential bucket a flag is decoded from the bit stream, determining if the values of the current bit level of all potential coefficients contains one non-zero entry or not.

The third step then deals with the potential to active transition at the coefficient level. For all potential coefficients in buckets with the flag from the second step set, the current bit is decoded from the bit stream. If the bit is 1, i.e., the coefficient transitions to the active state, then additionally the sign bit is decoded. The bit for potential coefficients in buckets for which the flag from the last step was not set are set to 0.

Finally, in the last step, the current bit for all active coefficients is decoded from the stream, completing the decoding of a bit-level of the current band. This decoding procedure is then repeated for all bands, blocks and slices and color components until the end of the bit-stream.

C. Wavelet and color reconstruction

The result of the band decoding is a sequence of blocks with 1+15 bit-tuples. Depending on how many bit-levels have been decoded, these tuples may only be known up to a certain precision, i.e., represent an interval of possible values. Such tuple are then replaced by middle of the corresponding interval and all tuples are converted to a a 16-bit number.

The blocks of coefficients (now represented by 16-bit numbers) are inherently linear data-structures. In the next step they are deserialized to 32 x 32 blocks, which are then copied into the image.

As the last part of the reconstruction, an inverse lifting scheme [17] of the Dubuc-Deslauriers-Lemire (4, 4) wavelet

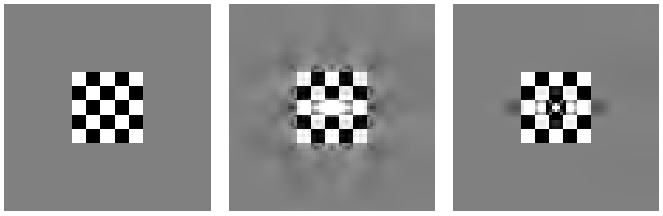

(a) Original image (b) 80 slices (c) 200 slices

Fig. 4. Critical test image: Size 73 x 73 with a checker-board pattern with fields of size 5x5. This image causes an integer overflow in the storage of the wavelet coefficients. Consequently, even the principally loss-less version with 200 slices exhibits artifacts.

transform [16] is carried out. In one dimension, the transform consists of two steps. In the first step, all coefficients c_k with even k are replaced by $c_k - \texttt{divround}(9(c_{k-1} + c_{k+1}) - (c_{k-3} + c_{k+3}), 32)$, where zero-extension is applied to coefficients lying outside of the image and $\texttt{divround}(x, y) := \texttt{floor}(x/y + 1/2)$. In the second step all odd-indexed coefficients c_k are replaced by $c_k + \texttt{divround}(9(c_{k-1} + c_{k+1}) - (c_{k-3} + c_{k+3}), 16)$. Notice that in the above formula c_{k-1} will always belong to the image. However if only c_{k+3}, or only c_{k-3}, or only c_{k-3} and c_{k-3}, do not belong to the image then the above cubic prediction formula is replaced by a linear prediction $c_k + \texttt{divround}(c_{k+1} + c_{k-1}, 2)$. In the remaining two cases (c_{k+1}, c_{k+3} do not belong to the image and c_{k-3} does or does not belong to the image) a constant prediction $c_k + \texttt{divround}(c_{k-1}, 1)$ is employed. The above transform is then carried out on rows and columns interchangeably, mutatis mutandis for 5 wavelet decomposition levels. After the wavelet transform, the 6 least significant bits of all coefficients are removed by replacing all coefficients c_k with $\texttt{divround}(c_k, 64)$. The result is clipped to 8-bit signed range $-128, \ldots, 127$.

Finally, for both color and grayscale images, the luminance channel Y is shifted by adding 128. For color images, the transformation $t_1 = C_r + \texttt{floor}(C_r/2)$, $t_2 = Y - \texttt{floor}(C_b/4)$, $R = Y + t_1$, $G = t_2 - \texttt{floor}(t_1/2)$, $B = t_2 + C_b * 2$ is then carried out. The resulting RGB channels are then clipped to $0, \ldots, 255$. The above transformation is similar to the usual $YCbCr$ to RGB transform, with values rounded to the nearest multiple of $\frac{1}{4}$.

Remark:

As mentioned in the previous sections, the dynamic range allocated for the wavelet coefficients is 15 bits (with an additional sign bit). The range of the color channel is essentially a 7 bit number (+ 1 additional sign bit). Prior to the wavelet transform, this number is multiplied by 64, hence the input of the wavelet transform is essentially a 13 bit (+1 sign bit). This means that the output of the wavelet transform is only stored correctly if the ∞ norm of the synthesis matrix is at most 4. However, a simple computation shows this not to be the case. Consequently, there are images which are not stored (and therefore not decoded) correctly due to this 'too small' dynamic range. An example of this integer overflow/underflow is depicted in Figure 4.

III. TGV based DjVu reconstruction

We can learn from the explanations in the previous section that, after inverting the lossless compression, a DjVu image layer provides a set of DDL $(4, 4)$ wavelet coefficients of the unknown, uncompressed image. As result of the data loss during compression, these coefficients are, however, only known up to a certain level of precision. The DjVu standard decompression accounts for that by estimating the true coefficients to be in the center of their admissible range, which is defined via the level of precision up to which each coefficient is known.

This choice, however, is somewhat arbitrary and our goal is to improve upon that. To this aim, we interpret the admissible range for each coefficient, which can be determined from the compressed file, as given data interval. This then yields a set of admissible wavelet data, henceforth denoted by D, such that the DDL $(4, 4)$ wavelet transform of the uncompressed image is guaranteed to be contained in this set.

Continuing on these lines, the decompression of a given DjVu image layer in fact amounts to choose an image such that the coefficients of its wavelet transform are contained in D. As mentioned above, standard DjVu decompression achieves this by just setting the first unknown bit to one and all others to zero, which corresponds to choosing the center points of the error intervals.

Our approach is to make a more sophisticated choice which is motivated by a predefined image model. This is achieved in the context of variational regularization for image processing: We regard an image as a function mapping from a rectangular domain to the reals (for grayscale images) or, more generally, to $\mathbb{R}^{N_c}$ (with $N_c = 3$ for color images). An image model is then realized via a regularization functional $\mathcal{R}$, mapping from the vector space of images to the positive reals, thereby assigning each image to a number which is the lower the better it fits to the underlying model. Consequently, defining W to be the DDL wavelet operator (performing five levels of decomposition), variational DjVu decompression amounts to obtain the reconstructed image as the solution of the minimization problem

$$\min_u \mathcal{R}(u) \quad \text{such that} \quad Wu \in D. \tag{1}$$

This corresponds to choosing, among all possible source image of the compressed DjVu file, the (not necessarily unique) one that best fits the image model.

Naturally, the regularization functional realizing the image model hence plays a crucial role for the quality of the reconstructed image as well as for the computational feasibility of such an approach. Many research has been devoted to find appropriate regularization functionals that are both computationally tractable and suitable for a large range of realistic images. The Total Variation (TV) functional [18] which essentially penalizes the one-norm of the image gradient is a popular choice. Regarding images a functions, a main advantage of TV is that it achieves derivative based regularization while still allowing jump discontinuities, which in practice yields sharp edges in the reconstructed images. From the computational viewpoint, convexity of TV is another strong advantage as

it allows, when combined with convex data constraints, the approximation of provably optimal solutions.

However, a well-known defect of TV regularization is the fact that it tends to produce piecewise constant reconstructions [19], [20], [21], which is infeasible for many realistic images. A straightforward way of overcoming this would for instance be to penalize the one-norm of the second order derivative instead of the first order one [22]. However, again regarding images as functions, this leads a class of possible reconstructions that cannot have jump discontinuities, which in practice corresponds to blurred edges.

The *Total Generalized Variation (TGV)* functional (of order k) [1], [23], allows to overcome the defect of TV while still allowing jump discontinuities. This is achieved in a convex setting via an optimal balancing between different orders of differentiation up to order k. In the second order case, it is defined as

$$\mathrm{TGV}^2_\alpha(u) = \min_v \alpha_1 \left\|\nabla u - v\right\|_{\mathcal{M}} + \alpha_0 \left\|\mathcal{E} v\right\|_{\mathcal{M}},$$

with $\|\cdot\|_{\mathcal{M}}$ being the Radon norm, i.e., an L^1-type norm. The balancing is done by subtraction of the vector (or matrix) field v, which in turn is penalized via a symmetrized gradient $\mathcal{E}v = \frac{1}{2}(\mathcal{J}v + (\mathcal{J}v)^T)$, with $\mathcal{J}v$ being the Jacobian. As v is chosen to minimize the sum of the two penalties, it can be expected to be zero in regions where the image is already constant, i.e., where $\nabla u = 0$, and to be equal to ∇u in regions where the image is almost linear, yielding a penalization of the Hessian $Hu = \mathcal{E}\nabla u$. By choosing $v = 0$ one observes that TGV is always less or equal to TV, hence still admits finite values in case of jump discontinuities.

Motivated by the above-mentioned advantages, we apply the second order TGV functional as regularization term for variational DjVu decompression. We now define the discrete model in detail: Images are considered as $\mathbb{R}^{N_c}$-valued functions ($N_c \in \{1, 3\}$) on a rectangular domain Ω, which we discretize via $\Omega = \{(i, j) \mid 1 \le i \le N_x, 1 \le j \le N_y\}$. Abusing notation, we carry out identification:

- Vector fields $u : \Omega \subset \mathbb{R}^2 \to \mathbb{R}^{N_c}$ are identified with $u \in U := \mathbb{R}^{N_x \times N_y \times N_c}$,
- matrix fields $v : \Omega \subset \mathbb{R}^2 \to \mathbb{R}^{N_c \times 2}$ are identified with $v \in V := \mathbb{R}^{N_x \times N_y \times N_c \times 2}$,
- tensor fields $w : \Omega \subset \mathbb{R}^2 \to \mathbb{R}^{N_c \times 2 \times 2}$ are identified with $w \in \mathbb{R}^{N_x \times N_y \times N_c \times 2 \times 2}$.

Lower case indices always index space dimensions and upper case indices always index range dimensions, e.g., $u = (u^c_{i,j})_{i,j,c}$ where $i = 1, \dots N_x$, $j = 1, \dots N_y$ and $c = 1, \dots, N_c$. Since the tensor fields are used to represent the symmetrized gradient $\mathcal{E}v$, they will be symmetric around the last two coordinates, i.e.,

$$(w)^c_{i,j} = \begin{bmatrix} w^{c,1,1}_{i,j} & w^{c,1,2}_{i,j} \\ w^{c,1,2}_{i,j} & w^{c,2,2}_{i,j} \end{bmatrix}.$$

Hence, they have a reduced degree of freedom and we identify

- Symmetric tensor fields $w : \Omega \subset \mathbb{R}^2 \to \mathbb{R}^{N_c \times 2 \times 2}_{\mathrm{sym}}$ with $w \in W := \mathbb{R}^{N_x \times N_y \times N_c \times 3}$.

Again abusing notation, we define pointwise norms $|\cdot|$ on vector and matrix fields as the pointwise Euclidean and Frobenius norms, respectively, e.g., $|u|_{n,m} = \left(\sum_{i=1}^{N_c} (u^i_{n,m})^2\right)^{1/2}$, and a pointwise norm on symmetric tensor fields as the pointwise Frobenius norm where the coordinated representing the symmetric information is counted twice, i.e.,

$$|w|_{n,m} = \left(\sum_{i=1}^{N_c} (w^{i,1}_{n,m})^2 + (w^{i,2}_{n,m})^2 + 2(w^{i,3}_{n,m})^2\right)^{1/2}.$$

For the approximation of the gradient and symmetrized gradient, we need forward and backward finite differences which, for a vector r of length N, are defined as

$$(\partial^+ r)_i = \begin{cases} r_{i+1} - r_i & \text{for } 1 \le i \le N-1 \\ 0 & \text{for } i = N \end{cases}$$

and

$$(\partial^- r)_i = \begin{cases} r_i - r_{i-1} & \text{for } 2 \le i \le N \\ 0 & \text{for } i = 1 \end{cases}$$

respectively. For a multi-dimensional array we define the forward and backward differences ∂^+_x, ∂^+_y and ∂^-_x, ∂^-_y along the x and y dimension accordingly, mapping $\mathbb{R}^{N_x \times N_y}$ to itself.

The gradient and symmetrized gradient operators for vector and matrix fields, respectively, are then given as

$$\nabla u = \left(\begin{bmatrix} \partial^+_x \\ \partial^+_y \end{bmatrix} \begin{bmatrix} u^1 & \dots & u^{N_c} \end{bmatrix}\right)^T$$

and

$$(\mathcal{E}v)^c = \left(\begin{bmatrix} \partial^+_x & 0 \\ 0 & \partial^+_y \\ \frac{1}{2}\partial^+_x & \frac{1}{2}\partial^+_y \end{bmatrix} \begin{bmatrix} v^{c,1} \\ v^{c,2} \end{bmatrix}\right)^T,$$

where the transposition is carried out pointwise in space. Denoting by $\|\cdot\|_1$ the ℓ^1 norm on $\mathbb{R}^{N_x \times N_y}$, the discrete approximation of the TGV functional is then given for $u \in U$ as

$$\mathrm{TGV}^2_\alpha(u) = \min_{v \in V} \alpha_1 \||\nabla u - v|\|_1 + \alpha_0 \||\mathcal{E} v|\|_1.$$

We further define the discrete DDL wavelet transform operator W (cf. Section II) and, given a DjVu compressed file, denote by D the set of admissible wavelet coefficients. The discrete optimization problem for variational DjVu decompression is then given as

$$\min_{Wu \in D} \mathrm{TGV}^2_\alpha(u). \tag{2}$$

This is a non-smooth but convex optimization problem and, as described in the next section, we will employ duality based methods to approximate an optimal solution.

Regarding well-posedness, we remark that the minimization problem (2) in fact is a special case of the abstract class of problems considered in [2]. In particular, the existence result [2, Proposition 3.1] guarantees existence of a solution even for a infinite-dimensional version of (2), and in particular we can ensure existence for the discretized problem.

We close this section with a remark regarding the operator wavelet operator W. A close inspection of Subsection II-C shows that the wavelet decomposition as implemented by the lifting scheme is not linear. This is due to the rounding-division function `divround()`. However, for all intents and purposes the resulting operator can be replaced by a linear operator,

where the rounding-division is replaced by the true division, i.e. $\texttt{divround}(x, y) := x/y$. This is the only concession which we make in modeling the DjVu processing pipeline, for the remainder of the paper. As we will show in the results section this replacement does not have a significant impact on the quality of the reconstructions.

IV. Reconstruction method

It is the goal of the section to derive a globally convergent algorithm that approximates an optimal solution of (2). To this aim, we employ the primal-dual algorithm of [11], which allows to efficiently solve convex-concave saddle-point problems of the form

$$\min_x \max_y (Kx, y) - F^*(y) + G(x),$$

with $F^*(y) := \sup_z (z, y) - F(z)$ being the convex conjugate of a function F, if both F^* and G are prox-simple, meaning that solutions to $\min_u \frac{1}{2}\|u-u_0\|_2^2+\lambda H(u)$ with $H \in \{F^*, G\}$ can be computed efficiently and fast. Note that, due to strict convexity and coercivity of the 2-norm, given any u_0, a unique solution to the last equation indeed always exists, and the corresponding solution mapping is called the proximal mapping of H. We will essentially follow the derivation of a JPEG 2000 decompression algorithm in [3]. At first note that TGV can be re-written as

$$\mathrm{TGV}_\alpha^2(u) = \min_v \|K_1(u, v)\|_{1,\alpha}$$

with

$$K_1 = \begin{bmatrix} \nabla & -\mathrm{id} \\ 0 & \mathcal{E} \end{bmatrix}, \quad \|(p, q)\|_{1,\alpha} = \alpha_1 \||p|\|_1 + \alpha_0 \||q|\|_1.$$

A straightforward computation shows that the convex conjugate of $\|\cdot\|_{1,\alpha}$ is given as

$$\|(p, q)\|_{1,\alpha}^* = \begin{cases} 0 & \text{if } \max\{\alpha_1 \||p|\|_\infty, \alpha_0 \||q|\|_\infty\} \le 1, \\ \infty & \text{else.} \end{cases}$$

The data constraint in (2) can be written by adding the convex indicator function $\mathcal{I}_D(Wu)$ to the objective function, where $\mathcal{I}_D(r) = 0$ if $r \in D$ and $\mathcal{I}_D(r) = \infty$ else.

The convex conjugate of $\mathcal{I}_D$ is then given as $\mathcal{I}_D^*(r) = \sup_{s\in D}(r, s)$. The reformulation of (2) is now carried out as follows:

$$\begin{aligned} &\min_{Wu\in D} \mathrm{TGV}_\alpha^2(u) \Leftrightarrow \min_{u,v} \|K_1(u, v)\|_{1,\alpha} + \mathcal{I}_D(Wu) \\ &\Leftrightarrow \min_{u,v} \max_{p,q,r} (K_1(u, v), (p, q)) - \|(p, q)\|_{1,\alpha}^* + (Wu, r) - \mathcal{I}_D^*(r) \\ &\Leftrightarrow \min_{u,v} \max_{p,q,r} (K(u, v), (p, q, r)) - F^*(p, q, r), \end{aligned}$$

with

$$K = \begin{bmatrix} \nabla & -\mathrm{id} \\ 0 & \mathcal{E} \\ W & 0 \end{bmatrix} \quad \text{and} \quad F^*(p, q, r) = \|(p, q)\|_{1,\alpha}^* + \mathcal{I}_D^*(r)$$

the convex conjugate of $F(p, q, r) = \|(p, q)\|_{1,\alpha} + \mathcal{I}_D(r)$. The last line of the above equivalence defines a saddlepoint problem that can be solved by the algorithm of [11] and, as can be deduced with standard convex analysis arguments [24], is equivalent to the original problem in the sense that, given $((u, v), (p, q, r))$ a solution to the saddle-point problem, u is an optimal solution of (2). The resulting algorithm is provided in Algorithm 1. There, the operators proj_{α_1}, proj_{α_0} result from the proximal mapping of $\|\cdot\|_{1,\alpha}^*$ and can be calculated explicitly as

$$(\mathrm{proj}_\lambda(s))_{n,m}^{c,i} = s_{n,m}^{c,i} / \max\{1, |s_{i,j}|/\lambda\}.$$

The operator $\mathrm{shrink}_{D,\sigma}$ results from the proximal mapping of $\mathcal{I}_D^*$ and can be calculated explicitly as

$$(\mathrm{shrink}_{D,\sigma}(r))_{n,m}^c = \begin{cases} r_{n,m}^c - \sigma o_{n,m}^c & \text{if } r_{n,m}^c > \sigma o_{n,m}^c \\ r_{n,m}^c - \sigma l_{n,m}^c & \text{if } r_{n,m}^c < \sigma l_{n,m}^c \\ 0 & \text{else.} \end{cases}$$

where $J_{n,m}^c = [l_{n,m}^c, o_{n,m}^c]$ defines the data constraint of the wavelet coefficient (n, m) of the color component c for the data set D. In contrast to the original implementation as provided in [11], we use an adaptive choice of the stepsizes σ and τ according to [3], which still ensures convergence of the algorithm while in practice allowing to overcome stepsize constraint $\sigma\tau\|K\|^2 \le 1$ provided in [11]. The adaptive choice is realized via the mapping $\mathcal{S}$, which is defined as

$$\mathcal{S}(\sigma\tau, \mathfrak{n}) = \begin{cases} \mathfrak{n} & \text{if } \sqrt{\theta\sigma\tau} \ge \mathfrak{n}, \\ \sqrt{\theta\sigma\tau} & \text{if } \sqrt{\sigma\tau} \ge \mathfrak{n} > \sqrt{\theta\sigma\tau}, \\ \sqrt{\sigma\tau} & \text{else.} \end{cases} \tag{3}$$

The parameter η defines the ratio between the primal and the dual step and was set to $\eta = 0.005$ for all experiments, as this accelerated convergence. The norm $\|\cdot\|_2$ in Algorithm 1 refers to the standard ℓ^2 norm over all pixels and the pointwise norm $|\cdot|$ is meant component-wise. The operators $\mathrm{div} : V \to U$ and $\mathrm{div}_2 : W \to V$ are defined as the negative adjoints of ∇ and $\mathcal{E}$, respectively, with respect to the standard inner product. As stopping criterion, we use the normalized primal dual gap

Algorithm 1 Algorithm for variational DjVu decompression

function TGV-DjVu(FILE)
  $D \leftarrow$ interval bounds from decoding of FILE
  $d \leftarrow$ centers of interval bounds, $u \leftarrow W^{-1}(d)$
  $v \leftarrow 0, \overline{u} \leftarrow u, \overline{v} \leftarrow 0, p \leftarrow 0, q \leftarrow 0, r \leftarrow 0$
  choose $\sigma, \tau > 0$, $\eta > 0$
  repeat
    $p \leftarrow \mathrm{proj}_{\alpha_1}(p + \sigma(\nabla\overline{u} - \overline{v}))$
    $q \leftarrow \mathrm{proj}_{\alpha_0}(q + \sigma\mathcal{E}\overline{v})$
    $r \leftarrow \mathrm{shrink}_{D,\sigma}(r + \sigma W\overline{u})$
    $u_+ \leftarrow u - \tau(-\mathrm{div}\, p + W^* r)$
    $v_+ \leftarrow v - \tau(-p - \mathrm{div}_2\, q)$
    $\overline{u} \leftarrow (2u_+ - u)$, $\overline{v} \leftarrow (2v_+ - v)$
    $\sigma_+ \leftarrow \eta\mathcal{S}(\sigma\tau, \frac{\|\|(u_+, v_+) - (u, v)\|\|_2}{\|\|K((u_+, v_+) - (u, v))\|\|_2})$
    $\tau_+ \leftarrow \sigma_+/\eta^2$
    $u \leftarrow u_+$, $v \leftarrow v_+$
  until Stopping criterion fulfilled
  return u_+
end function

defined in [3], which is for our setting given as

$$\begin{aligned}\mathcal{G}(u,v,p,q,r) = \tfrac{1}{N_x N_y N_c}\Big(&F(K(u,v)) + \mathcal{D}(Wu,r) \\ &+\gamma\|u\|_2\|\operatorname{div}^2\tilde{q} - W^*r\|_2 \\ &+\sum_{(i,j,c)} \tfrac{l^c_{i,j}+o^c_{i,j}}{2}(r)^c_{i,j} + |\tfrac{o^c_{i,j}-l^c_{i,j}}{2}(r)^c_{i,j}|\Big)\end{aligned} \tag{4}$$

where

$$\mathcal{D}(s,r) = \sum_{s^c_{i,j}\notin J^c_{i,j}} \gamma|(r)^c_{i,j}|\max\{s^c_{i,j}-o^c_{i,j}, l^c_{i,j}-s^c_{i,j}\},$$

$\tilde{q}_n = \beta_n q_n$, with $\beta_n := \frac{\alpha_1}{\max(\alpha_1, \|\operatorname{div} q_n\|_\infty)}$ and $\gamma > 1$. Summarizing the variables at iteration n by $x_n = (u_n, v_n)$ and $y_n = (p_n, q_n, r_n)$, it was shown in [3] that, $\mathcal{G}(x_n, y_n) \to 0$ as $n \to \infty$ and, after finitely many iterates,

$$0 \le F(Kx_n) + \mathcal{D}(Wu_n, r_n) - \mathrm{TGV}^2_\alpha(\hat{u}) \le \mathcal{G}(x_n, y_n),$$

with $\hat{u}$ being an optimal solution to the variational decompression problem (1). In particular, $\mathcal{G}(x_n, y_n) = 0$ if and only if (x_n, y_n) solves the saddle-point problem equivalent to (2).

V. Numerical evaluation

The purpose of this section is to evaluate the proposed method numerically and compare with existing techniques. As, to the best knowledge of the authors, there are no methods available that are particularly tailored towards DjVu image decompression, we compare to custom modifications of related approaches as well as state-of-the-art denoising methods. Regarding the latter, we stress that the meaningfulness of such a comparison is naturally limited to assessing the extend to which these methods can be "misused" for postprocessing, as they are originally designed for Gaussian noise removal and no decompression-specific modifications were implemented. The following techniques were used for comparison:

Standard decompression: The standard decompression is the result provided by the reference implementation [14].

TV-based decompression: In addition to the TGV image model, we also test the total variation (TV) model. To this aim, the TGV^2_α functional in (2) is replaced by $\mathrm{TV}(u) = \|\nabla u\|_1$. For numerical solution, Algorithm 1 was adapted accordingly.

Non-local means filtering (NLM): The main idea of NLM is to achieve image denoising with non-local pixel-averaging, weighted by similarity of patches around the pixels, see [25]. In our experiments we have employed the implementation provided by one of the original authors of NLM [26] (channel-wise for color images).

Block-matching and 3D filtering (BM3D): As NLM, also BM3D [27] is patch-based, but filtering is carried on matching patches using both spatial smoothing via appropriate 2D transforms and a smoothing across transformed patches by a thresholding of Haar wavelet coefficients. For our experiments we have employed the (closed source) implementation provided by the original authors of BM3D [28].

Non-local total variation (NLTV): The non-local total variation functional $\mathrm{NLTV}(u) = \sum_i \Big(\sum_j (u_i - u_j)^2 w_{i,j}\Big)^{1/2}$, as proposed in [29], was employed in [5] for wavelet inpainting. Translated to the setting of this paper, this comprises the solution of $\min_{Wu\in D} \mathrm{NLTV}(u)$, where the set D is a product-set of sets which are singletons or the whole set of real numbers $\mathbb{R}$. In the light of image decompression this can be interpreted as either knowing the related wavelet-coefficients exactly (singleton case) or not at all (whole $\mathbb{R}$ case). Simulating this situation, we provide a comparison of our method to NLTV regularization using the reference implementation provided by one of the authors [30], which uses an iterative update of the weights $(w_{i,j})_{i,j}$.

A. Results and Discussion

For NLM, BM3D and NLTV standard parameters as given in the reference implementations were employed. For the TV-variant of the proposed method no user-provided parameters are necessary. In the TGV-version, one user-provided parameter, namely the ratio $\frac{\alpha_0}{\alpha_1}$ determining the trade-off between first and second order derivative information, is necessary and was fixed to $\sqrt{2}$, which has already been confirmed to be a good choice for different imaging applications [2], [31].

A crucial a-priori information for the proposed algorithm is the knowledge of the admissible intervals for the wavelet-coefficients, cf. D in (2). This is virtually equivalent to a decoding of the bitstream information of a DjVu-file. We have implemented such decoding routine in MATLAB, relying of the DjVu standard in version 2 and 3. For certain details of the implementation of the ZP-codec we have relied on the reference implementation by djvulibre library, cf. [14]. The source code of our decoder together with the TV and TGV reconstruction code and a script allowing to reproduce the results of Figure 6 below will be available online at the author's homepage.

A first example of the effect of our method on the three-layer DjVu page used in the introduction is shown in Figure 1. There, both the fore- and background layer was compressed and afterwards reconstructed by the proposed methods. The results show an improvement of image quality compared to standard decompression, both for the photographic part and the pie chart.

In Figure 6 we provide a qualitative evaluation of the algorithm on three images comparing standard as well as TV and TGV based DjVu decompression with postprocessing by NLM and BM3D denoising. The TV and TGV based reconstruction was obtained using $\mathcal{G}(u,v,p,q,r) < 0.2$, with $\mathcal{G}$ as in (4) as stopping criterion. Two photographic and one synthetic clip-art example and are presented. In the djvulibre library we have found two values of 80 and 100 slices as default values for the compression of images and we show the mildly overcompressed case of 80 slices. Visual inspection shows that the proposed TGV-based method again allows to significantly improve upon standard decompression. This is especially evident in the round reflection part of the "Leaf" example, the details of the eye structure in the "Alina" example as well as in the interfaces of the "Eye-clipart" example. A postprocessing with NLTV and BM3D filtering also improves image quality, but some compression artifacts remain. In contrast to that, the TV-based variant is able to remove all such artifacts and keeps edges sharp, however, at the cost of

Fig. 5. Top: Standard decompression of DjVu file, bottom: TGV based decompression of same file. Left: Entire page, right: Close up-views.

degrading image quality by introducing regions with piecewise constant values (the staircasing effect). Enforcing piecewise smoothness, as done with the TGV-based method, leads to sharp edges with natural transitions in-between. For cartoon-like images, such as the "Eye-clipart", this allows almost perfect reconstruction. Due to the hart wavelet constraints obtained from the compressed file on the other hand, small details in the photographic images are not over-smoothed.

These qualitative differences in the reconstruction, however, are not well captured by the standard image similarity measures peak signal-to-noise ratio (PSNR) and structure similarity index (SSIM) [32], whose values are very similar and do not reflect the visual quality of the reconstructions.

At last, Figure 7 compares different regularization approaches for improving upon the n-term approximation of a given image using 5% of the coefficients of the five-level DDL $(4, 4)$ wavelet transform. To account for the larger set of admissible images, resulting from unbounded data intervals with the n-term approximation, the slightly more restrictive stopping criterion $\mathcal{G}(u, v, p, q, r) < 0.1$, again with $\mathcal{G}$ as in (4), was used for the TGV reconstructions. The results are presented in Figure 7. As in the case of color image decompression, the presented method is able to reliably recover sharp edges and smooth transitions. Wavelet artifacts with the zero-fill wavelet reconstruction are more severe this time, and consequently, the visual improvement with the TGV based method is even stronger. Again, however, quantitative evaluation gives comparable results indicating a weak relation of error measures and visual image quality. The NLTV based method also remove wavelet artifacts, but introduces new artifacts, such as around the parrots eye. This might be explained by the fact that NLTV method uses an iterative update of the weights, a procedure which makes the overall problem non-convex.

Fig. 7. Simulated decompression with n-term wavelet approximation (5% of coefficients). From Left to right: Inverse DWT, NLTV, TGV. [PSNR/SSIM]: Standard [29.6/0.87], NLTV [27.3/0.85], TGV [29.3/0.88]

References

[1] K. Bredies, K. Kunisch, and T. Pock, "Total generalized variation," *SIAM J. Imaging Sci.*, vol. 3, no. 3, pp. 492–526, 2010.

[2] K. Bredies and M. Holler, "A TGV-based framework for variational image decompression, zooming and reconstruction. Part I: Analytics," *SIAM J. Imaging Sci.*, vol. 8, pp. 2214–2850, 2015.

[3] ——, "A TGV-based framework for variational image decompression, zooming and reconstruction. Part II: Numerics," *SIAM J. Imaging Sci.*, vol. 8, pp. 2851–2886, 2015.

[4] Y.-W. Wen, R. H. Chan, and A. M. Yip, "A primal-dual method for total variaton-based wavelet domain inpainting," *IEEE Trans. Image Process.*, vol. 21, no. 1, pp. 106–114, 2011.

[5] X. Zhang and T. F. Chan, "Wavelet inpainting by nonlocal total variation," *Inverse Probl. Imag.*, vol. 4, no. 1, pp. 191–210, 2010.

[6] T. F. Chan, J. Shen, and H.-M. Zhou, "Total variation wavelet inpainting," *J. Math. Imaging Vision*, vol. 25, no. 1, pp. 107–125, 2006.

[7] S. Zhong, "Image coding with optimal reconstruction," in *ICIP, IEEE*, vol. 1, 1997, pp. 161–164.

[8] F. Alter, S. Durand, and J. Froment, "Adapted total variation for artifact free decompression of jpeg images," *J. Math. Imaging Vision*, vol. 23, no. 2, pp. 199–211, 2005.

[9] K. Bredies and M. Holler, "A total variation–based JPEG decompression model," *SIAM J. Imaging Sci.*, vol. 5, no. 1, pp. 366–393, 2012.

[10] [Online]. Available: http://sourceforge.net/projects/djvu/files/DjVuLibre/

[11] A. Chambolle and T. Pock, "A first-order primal-dual algorithm for convex problems with applications to imaging," *J. Math. Imaging Vision*, vol. 40, pp. 120–145, 2011.

[12] P. Haffner, P. G. Howard, P. Simard, Y. Bengio, Y. Lecun *et al.*, "High quality document image compression with djvu," *Journal of Electronic Imaging*, vol. 7, no. 3, pp. 410–425, 1998.

[13] [Online]. Available: http://www.djvuzone.org

[14] [Online]. Available: http://djvu.sourceforge.net/

[15] J. Morrison, "Iff standard," 1985. [Online]. Available: http://www.digitalpreservation.gov/formats/fdd/fdd000115.shtml

[16] G. Deslauriers, S. Dubuc, and D. Lemire, "Une famille d'ondelettes biorthogonales sur l'intervalle obtenue par un sch àema d'interpolation it àerative," *Ann. Sci. Math. Quéebec*, vol. 23, pp. 37–48, 1999.

[17] W. Sweldens, "The lifting scheme: A custom-design construction of biorthogonal wavelets," *Appl. Comput. Harmon. Anal.*, vol. 3, no. 2, pp. 186–200, 1996.

[18] L. Rudin, S. Osher, and E. Fatemi, "Nonlinear total variation based noise removal algorithms," *Phys. D*, vol. 60, pp. 259–268, 1992.

[19] M. Nikolova, "Local strong homogeneity of a regularized estimator," *SIAM J. Appl. Math*, vol. 61, pp. 633–658, 2000.

[20] V. Caselles, A. Chambolle, and M. Novaga, "The discontinuity set of solutions of the TV denoising problem and some extensions," *Multiscale Model Simul*, vol. 6, pp. 879–894, 2007.

[21] W. Ring, "Structural properties of solutions to total variation regularization problems," *Esaim Math Model Numer Anal*, vol. 34, pp. 799–810, 2000.

[22] W. Hinterberger and O. Scherzer, "Variational methods on the space of functions of bounded hessian for convexification and denoising," *Computing*, vol. 76, no. 1, pp. 109–133, 2006.

Fig. 6. Comparison of TGV regularized decompression with different postprocessing techniques. From left to right: Standard, NLM, BM3D, TV, TGV. [PSNR/SSIM]: Leaf: Standard [31.0/0.91], NLM [31.5/0.92], BM3D [31.3/0.92], TV [30.5/0.91], TGV [31.1/0.92], Alina: Standard [32.3/0.92], NLM [32.6/0.92], BM3D [32.5/0.92], TV [30.3/0.86], TGV [32.0/0.91], Eye-clipart: Standard [34.4/0.90], NLM [36.1/0.92], BM3D [35.5/0.92], TV [34.9/0.91], TGV [35.1/0.94]. Top and middle images "Leaf" [33] and "Alina" [34] licenced under CC BY-SA 2.0 (https://creativecommons.org/licenses/by-sa/2.0/). Bottom clipart "Eye-clipart" [35] licenced under CC0 (https://creativecommons.org/about/cc0).

[23] K. Bredies and M. Holler, "Regularization of linear inverse problems with total generalized variation," *J. Inverse Ill-Posed Probl.*, vol. 22, no. 6, pp. 871–913, 2014.

[24] I. Ekeland and R. Témam, *Convex Analysis and Variational Problems*. SIAM, 1999.

[25] A. Buades, B. Coll, and J.-M. Morel, "A non-local algorithm for image denoising," in *CVPR*, vol. 2. IEEE, 2005, pp. 60–65.

[26] [Online]. Available: http://www.mathworks.com/matlabcentral/fileex change/13176-non-local-means-filter

[27] K. Dabov, A. Foi, V. Katkovnik, and K. Egiazarian, "Image denoising by sparse 3-d transform-domain collaborative filtering," *IEEE Trans. Image Process.*, vol. 16, no. 8, pp. 2080–2095, 2007.

[28] [Online]. Available: http://www.cs.tut.fi/ foi/GCF-BM3D/

[29] G. Gilboa and S. Osher, "Nonlocal operators with applications to image processing," *Multiscale Model Simul*, vol. 7, no. 3, pp. 1005–1028, 2008.

[30] [Online]. Available: http://math.sjtu.edu.cn/faculty/xqzhang/

[31] F. Knoll, K. Bredies, T. Pock, and R. Stollberger, "Second order total generalized variation (TGV) for MRI." *Magn. Reson. Med.*, vol. 65, no. 2, pp. 480–491, 2011.

[32] Z. Wang, A. C. Bovik, H. R. Sheikh, and E. P. Simoncelli, "Image quality assessment: from error visibility to structural similarity," *IEEE Trans. Image Process.*, vol. 13, no. 4, pp. 600–612, 2004.

[33] Steve-h, "Oak leaves and bokeh." [Online]. Available: https://www.flickr.com/photos/sbh/6802942537/

[34] I. P. Gheorghita, "Alina's eye." [Online]. Available: https://www.flickr.com/photos/angel_ina/3201337190/

[35] OpenClipartVectors, "Eye clipart." [Online]. Available: https://pixabay.com/de/auge-wimperntusche-make-up-iris-149604/